
Article

Monitoring the microseismicity through a dense seismic array and a similarity search detection technique: application to the gas-storage site of Collalto, North Italy.

Antonio Scala¹, Guido Maria Adinolfi², Matteo Picozzi^{1,*}, Francesco Scotto di Uccio¹, Gaetano Festa¹, Grazia De Landro¹, Enrico Priolo³, Stefano Parolai³, Rosario Riccio⁴ and Marco Romanelli³

¹ Department of Physics "Ettore Pancini", University of Napoli Federico II, Italy;

² Dipartimento di Scienze e Tecnologie, Università degli Studi del Sannio, Italy

³ Istituto Nazionale di Oceanografia e di Geofisica Sperimentale - OGS, Italy

⁴ Istituto Nazionale di Geofisica e Vulcanologia, Sezione Napoli - Osservatorio Vesuviano, Italy

* Correspondence: matteo.picozzi@unina.it;

Abstract: Seismic monitoring in areas where induced earthquakes could occur is a challenging topic for seismologists due to generally very low signal to noise ratio. Therefore, the seismological community is devoting several efforts to the development of high-quality networks around the areas where fluid injection and storage and geothermal activities take place, also following the national induced seismicity monitoring guidelines. The use of advanced data-mining strategy, such as template matching filters, auto-similarity search and deep-learning approaches is recently further fostering such a monitoring enhancing the seismic catalogues and lowering the magnitude of completeness of these areas. In this framework, we carried out an experiment where a small-aperture seismic array was installed around the gas reservoir of Collalto, in North Italy. The continuous velocimetric data, acquired for 25 days, were analysed through the application of the optimized auto-similarity search technique FAST. The array was conceived as a cost-effective network, aimed at integrating, right above the gas storage site, the permanent high-resolution Collalto Seismic Network. The analysis allowed to detect micro-events down to magnitude $M_l = -0.4$ within a distance of ~15km from the array. Our results confirmed that the system based on the array installation and the FAST data-analysis might contribute to lower the magnitude of completeness around the site of about 0.7.

Keywords: Induced seismicity Monitoring; seismic arrays; sensor network technology; microearthquake detection;

1. Introduction

Monitoring the seismicity in areas of underground hydrocarbon exploitation and fluid injection and storage is a crucial task considering the significant socio-economic implications in case of induced earthquakes [1]. Seismic monitoring aims to characterize the spatio-temporal evolution of the seismicity in a sub-surface volume where industrial exploitation activities take place with the two following goals: i) discriminating the natural seismicity from the anthropogenic one (i.e., induced), ii) intercepting variations in the background seismicity rate that, if needed, will guide the re-modulation, interruption, and restart of industrial activities. Indeed, tracking the microseismicity in time after fluid injection and accurately locating it can allow one to detect pore pressure changes and intercept migration fluid patterns [2].

An exhaustive review of concepts, methods, and physical basis concerning the monitoring of induced seismicity, possibly deploying small aperture seismic arrays, is provided by

[3] and references therein. In this framework, [4] realized a feasibility study for seismic networks aiming to monitor the induced seismicity according to the performance requirements in the Italian guidelines [5]. Such a study considered several network layouts, with different geometries and station densities, also including the use of seismic arrays with a maximum aperture size of 1 km. The results indicate that, for low noise levels, integrating of seismic networks with small-scale arrays can achieve a magnitude detection threshold close to Mw 0 and small location errors (i.e., a few hundreds of meters for depths down to 8 km).

For this reason, during the last years, efforts from the seismological community have focused on the development of cost effective seismic sensors that can be combined with high-quality observing systems. Furthermore efforts have been done in the application of innovative data-mining strategies for improving the detection capability.

An example of a high-sensitivity network is the one deployed around the Collalto underground gas storage (UGS) in north-eastern Italy [6]. The Collalto seismic network (Rete Sismica di Collalto, RSC) aims at monitoring the natural and induced seismicity potentially related to the industrial activity of the Collalto gas storage facility. It is composed of ten seismological stations equipped with borehole seismometers with periods varying between 10 s and 120 s operating at a sampling rate of 200 Hz, and accelerometric sensors at the surface of five sites. This network is managed by Istituto Nazionale di Oceanografia e di Geofisica Sperimentale- OGS on behalf of Edison Stoccaggio S.p.A., that is the holder of the storage concession, and it has been the first case of industrial seismic monitoring in Italy managed by a public research institute. The RSC is fully operating since the 1st January 2012, and it represented an important experience for the Italian guidelines for monitoring the industrial activities associated with underground resource exploitation, that were developed after the destructive earthquake that struck the Emilia region in 2012 [5]. The OGS guarantees the seismic (real-time and off-line) monitoring and network maintenance service, as well as any related research activity, delivering full data and transparent information through the RSC website (rete-collalto.crs.inogs.it). Publicly available data include full waveform data and the earthquake catalogue, which is updated every six months. More details about the network deployment and features can be found in [6].

The Collalto gas field is a natural, depleted reservoir with a working gas storage capacity of approximately 600 million standard m³ (total capacity of more than 900 million standard m³) covering an area of almost 89 km² [7]. The field is equipped with 17 active wells through which the gas is seasonally injected into the reservoir during the November-March period and extracted during the April-October period [6,8]. In ten years of operation, the Collalto seismic network recorded thousands of microearthquakes of natural origin in the surrounding areas, reaching a completeness magnitude M_c for the whole area of 0.6 and 1.2 for the local [8], and moment [9] magnitude, respectively, and of 0.1 for a smaller region around the reservoir [10].

The efficiency of seismic monitoring can be further enhanced by data-mining approaches, capable of enriching earthquake catalogues, lowering the M_c threshold near to 0 or below, and hence allowing to better investigate the mechanical features of the spatio-temporal seismicity evolution. Most of these methods [11-14] are generally referred to as template matching. They detect micro-events within a continuous data stream through cross-correlation of the waveforms associated with some previously identified earthquakes. As an example of the efficiency of this approach, [15] retrieved an extended catalogue of ~3500 earthquakes for the 2013 induced seismic sequence at the Castor injection platform offshore Spain, which includes three earthquakes of magnitude 4.1. This final catalogue significantly improved the official IGN and Ebro catalogues, reporting 536 and 982 earthquakes respectively. Thanks to this catalogue [15], the authors were able to study the

progressive fault failure and unlocking, triggered by pore pressure diffusion and characterized by migration of seismicity away from the injection point. Moreover, the detection through the recognition of some peculiar seismic waveform features is nowadays being developed more and more by means of advanced deep learning algorithms [16].

Similarity search can be carried out also without the use of template events, using auto-correlation techniques that correlate different portions of the continuous data stream [17-21]. These methods are particularly efficient in areas characterized by a low level of seismicity with few events available in seismic catalogues. Nevertheless, the computational costs are much more expensive due to the need for mutual comparison between all data portions. The FAST technique (Fingerprinting and Similarity Thresholding, [22-23]) represents an optimized auto-correlation approach, based on the compression of waveforms in key discriminative features, using binary fingerprints, and the a priori grouping of similar fingerprints to reduce the order of magnitude of the performed comparisons. The FAST technique playbaced on the Hector Mine earthquake (1999, Mw 7.1, [24]) revealed an intense foreshock sequence with 50 detected events with a minimum magnitude of -0.4. Recently, the same approach was applied to the Southern Italy, Rocca San Felice sequence (3-6 July 2020, maximum magnitude $M_L=3.0$), allowing to increase of factor 10 the number of detected events while lowering of about 1 point in magnitude the completeness threshold when compared to the released Irpinia Seismic Network [25-26].

In this work, we aim to show how and to what extent a small aperture, low-cost seismic array combined with an advanced microseismicity detection technique can locally improve the performance of a permanent, high-quality, less-dense seismic network, enhancing the local earthquake catalogue and hence allowing to better characterize the spatio-temporal evolution of the micro-seismicity in the vicinity of a gas-storage site. We used the data collected during an experiment that integrated the array monitoring system for induced seismicity application, proposed by [4], with the data-mining approach implemented in the FAST technique. For this purpose, the installed array, with a 2 km maximum aperture, was composed by eight seismic stations located in the area nearby the gas storage site in Collalto. The temporary network was installed in winter time and was operative for about one month.

We first describe the geology of the investigated area, then we provide details about the experimental and methodological setups. Second, the results relevant to the number of detected events and their features will be presented and discussed. Finally, conclusions are presented.

2. Experiment

2.1. Seismotectonic setting

The underground gas storage of Collalto is located in north-eastern Italy, within the Adria-European collision zone where the Plio-Quaternary front of the Southern Alps is still active. The main tectonic structures are related to the origin of the SSE-verging Neogene-Quaternary eastern South-Alpine chain from the Adria-European continental margin collisions [27-28]. Thrusts and foreland folds (from Serravallian to Messinian) with S-vergence and WSW-ENE trends show an imbricate fan geometry with the main compressive stress axis oriented along NNW-SSE direction. The age and the activity of the thrust sheet migrated from north to south along the eastern Southern Alps showing the external younger thrust front in the foothill range of the mountain belt or buried in the foreland deposits, as in the Venetian region [28-29]. The Collalto gas storage is a stratigraphic/structural geological trap along the Montello anticline with an area of about

10 × 2.5 km². Several productive reservoirs, made up of calcareous sandstone with shales (Arenaria of Vittorio Veneto Formation) with a few meters thick, are located at depth of 1200-1400 m [8, 30]. The Montello-Conegliano thrust is part of the active, compressive external front of the eastern Southern Alps and it is bounded by the Bassano-Cornuda thrust to E, the Cansiglio thrust to NE, the Bassano-Valdobbiadene to N, and the Arcade thrust to S (Figure 1) [8,29]. The activity of these structures is testified by geological, geodetic, and seismological studies showing a compression rate of 1-2 mm/yr [31], according to N-S or NNW-SSE convergence and a low magnitude ($M < 4$) instrumental seismicity [6,8]. The active thrusts are kinematically independent and are rooted in the mid-crust (15-20 km) as evidenced by seismic profiles and seismicity [27].

In historical times, the Montello area (Figure 1) was hit by several earthquakes with $I_0 > 4$. Intermediate size earthquakes, such as the 1789, 1859, 1860, 1900, and 1966 events ($I_0 < 6-7$) can be associated to Montello-Conegliano seismogenic source (CPT15, [32]). The most destructive earthquake, the 1695 Asolano earthquake ($I_0 = 10$), occurred eastward and can be related to the activity of the Bassano-Cornuda thrust [28]. The instrumental seismicity of the last 50 years is moderate and occurred at depths of 15-20 km with magnitude < 4.5 (Figure 1). The fault plane solutions show reverse to strike-reverse kinematics. Since the end of 2011, the dense Collalto Seismic Network (RSC, Figure 1), deployed around the underground gas storage to monitor the associated industrial activities, has significantly improved the capability to detect the seismicity, lowering the regional and national monitoring thresholds below $M_I 1.0$. [8] show that the seismicity depicts the Montello-Conegliano active thrust as a gently NE-dipping plane, locally interrupted by minor faults, with earthquakes located at 5-13 km depth. In 6 years (2012-2017), [8] analysed 1635 earthquakes with $-0.8 \leq M_L \leq 4.5$ with strongest events located north-eastward, outside the principal monitored region, a 20 km wide square area denoted as the area A in [6] (see the smallest red dashed square in Figure 1). The largest events are spatio-temporally clustered in seismic sequences occurred near Sedico-Belluno, Vidor-Valdobbiadene, Cavaso del Tomba-Segusino (with $3.3 < M_{max} < 3.8$) and in the Pieve di Soligo, Tarzo-Vittorio Veneto and Alpagio areas (with $2.0 < M_{max} < 3.0$; Figure 1). The 2012-2017 earthquake catalogue reported in [8] revealed that no earthquake occurred in the volume surrounding the Collalto gas reservoir for a spatial range of 3 km, in the “inner domain” as described by the protocols stated by the Italian Ministry of the Economic Development (MiSE) monitoring guidelines [5]. Here, no seismicity is located at depths shallower than 5 km and within 13 km from the gas storage boundary (“external domain”); moreover, the seismicity recorded in 6 years has a magnitude smaller than 2.0, except for one event. It is important to note that the Collalto seismic network ensures a high detection capability for the area providing a completeness magnitude ranging from $M_I 0.1$ to $M_I 0.6$ inside the extended domain [8-10].

Different ideas exist about the seismic potential of the fault structures forming the compressive external front of the eastern Southern Alps. In particular, the seismic role of the Montello-Conegliano thrust is still debated as well as its fault plane continuity or segmentation. For some authors [28, 33-34], it is capable to originate earthquakes with $M > 6.5$ based on surface geological and structural data, while it can be characterized by creeping behaviour with small inter-seismic periods as hypothesized by other authors based on rheological modeling [35], and strain-rate or seismicity observations [8,31].

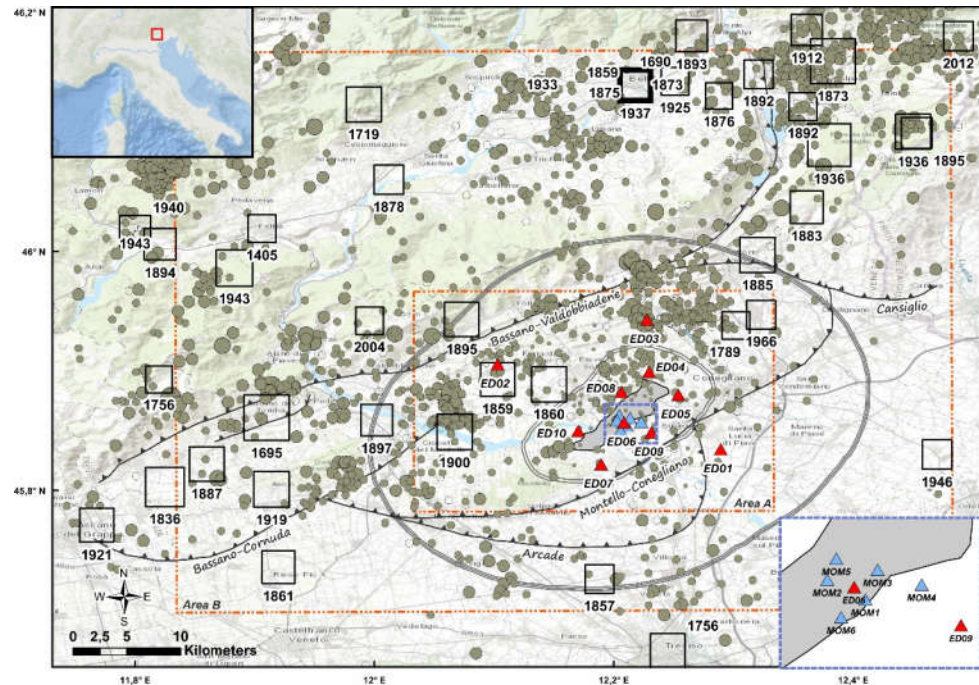


Figure 1. Epicentral location map of seismicity recorded by RSC (red triangles) in the period 01/01/2012-29/03/2021 (<http://retcollalto.crs.inogs.it/DATI/Localizzazioni/H71/fri/eventi-sismici-full-period.txt>). The magnitude of earthquakes (green circles) ranges between -0.9 to 3.8. The Collalto array is reported with blue triangles. The Collalto underground gas storage is shown in grey with the internal (two grey lines) and extended domain (three grey lines) areas. The monitoring areas A and B according to Priolo et al. (2015) are highlighted with dashed red lines. Historical seismicity with $I_0 > 4$ is reported (CPT15, [32]). Thrust faults of the compressive external front of the eastern Southern Alps are displayed according to [28].

2.1. Experimental setting

We designed the temporary array field experiment in the Collalto underground gas storage area to test its potential in detecting natural/induced micro-seismicity (Figure 2a). The objectives of the field experiment are: 1) to design and test a prototype implementation of a small dimension seismic array integrated within the Collalto seismic network; 2) to assess the performance the seismic array during the monitoring experiment when combined with modern powerful algorithms to detect micro-seismicity signals buried into ambient noise.

For the Collalto experiment, we designed a six-component (6C) seismic array made up of 6 smart seismic stations (MOMA, Figure 2b) capable of recording the ground motion with high resolution and real-time data transfer to a data acquisition centre, complemented by two stations of the RSC (ED06 equipped with a 120 s broad-band velocimeter at 5 m depth; ED09 equipped with an extended band seismometer at 14.6 m depth.) Each MOMA station is equipped with a 6C high dynamic range (32-bit) A/D-converter with SeedLink data transmission protocol (latency < 0.3 sec) capability, a 3C geophone (4,5 Hz), and a 3C MEMS accelerometer. Since in this work we are interested to detect low-amplitude micro-earthquakes signals, almost fully buried into the noise, only the velocimetric data are analysed. The data are recorded in MiniSeed format and stored on an internal compact memory flashcard. Each seismic station is equipped with a 12 V solar panel that ensures the recharge of a battery and an antenna for the radio communication to a local control system (Figure 2c). The MOMA seismic station was designed and manufactured by RISS

company (Realtime Innovative Solutions for Seismology), an academic spin-off of the Physics Department of the University of Napoli Federico II.

The seismic acquisition started on 7 January 2019 and lasted approximately one month. The installation sites were carefully chosen in order to get: 1) an adequate homogeneous coverage of the area of the underground gas reservoir reducing the interstation distances with respect to the RSC 2) a small azimuthal gap. All the stations were positioned within a radius of 2 km over the gas field area following an irregular geometry (Figure 2a).

We remind that both RSC stations are equipped with borehole instruments (ED06 has a 120 s broad-band velocimeter at 5 m depth; ED09 has an extended band seismometer at 14.6 m depth). Those stations sample data at 200 Hz. For the MOMA stations, the sampling rate was set at 250 Hz.

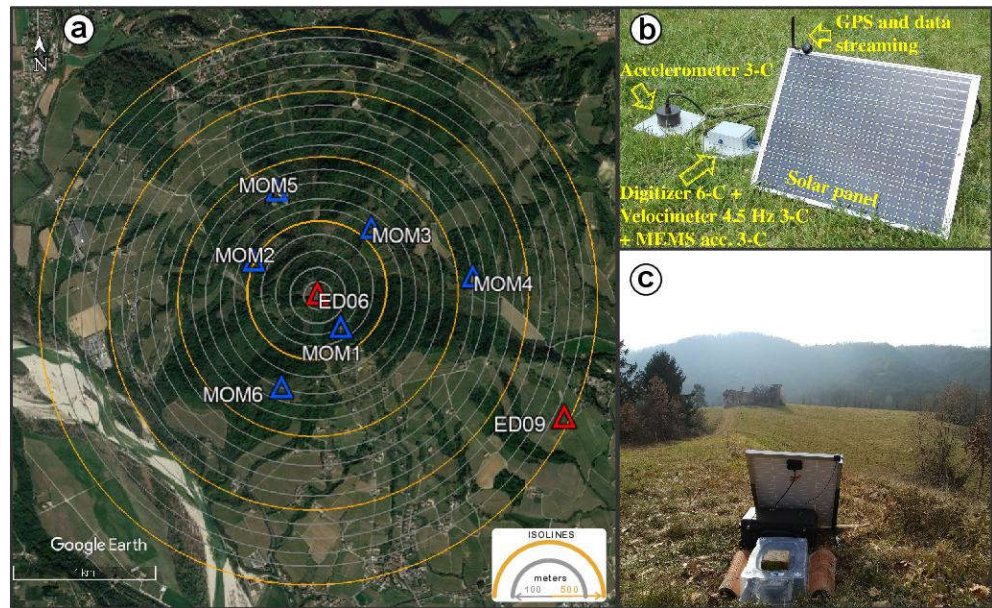


Figure 2. (a) Geometry of the Collalto array deployed in the Susegana (TV) municipality for the field experiment. The RSC and MOMA stations are represented by red and blue triangles, respectively. (b) Example of MOMA station configuration equipped with a 3C geophone (4.5 Hz), a 3C MEMS accelerometer. An additional external accelerometer might be added but it was not installed during this experiment. The seismic station is also equipped with a 12 V solar panel, GPS and radio antennas for communication to a local control system. (c) Example of field seismic station (MOM3) installed during the Collalto experiment..

3. Detection technique

To detect micro-earthquakes at the level of the seismic noise, we applied the FAST technique (Fingerprint And Similarity Thresholding, <https://github.com/stanford-futuredata/FAST> [24]) to the 25 days (from 7 to 31 January 2019) of continuous velocity data stream recorded during the experiment.

FAST is an uninformed self-similarity technique that converts time-domain waveforms into fingerprints, containing key discriminative features of earthquakes, and then performs an optimized similarity search to individuate couples of similar fingerprints. FAST features good performances both in computational efficiency and in detection sensitivity since it can reach the accuracy of autocorrelation methods while requiring lower runtime [24-25]. The advantage of using FAST is that it does not require templates

to search for similar events. Hence, it is particularly efficient in areas characterized by low seismicity, such as the gas-storage area of Collalto considered in this study.

The FAST workflow consists of four steps: a) data pre-processing; b) feature extraction, in which time series are compressed into binary fingerprints; c) similarity search, with similar fingerprints gathered in a database; d) network association, where single station detections are bound, and post-process analysis, where false events are discarded and the magnitude of the detected earthquakes is estimated.

In the pre-processing phase (Block 1 in the workflow of Figure 3), gaps and zero in the data stream are replaced with Gaussian uncorrelated noise. Moreover, the signal at all the stations is bandpass filtered between 1 and 20 Hz using a 2-poles acausal Butterworth filter and decimated to 50 Hz to dump the high frequency noise and improve computational efficiency.

In the feature extraction phase (Block 2 in Figure 3), 12.4 s long signals from single components are converted into spectrograms where each spectrum is built for 6.0 s of signal with a shift of 0.2 s, and the frequency range 1-20 Hz is subdivided in 32 equally spaced bins. The resulting spectrogram has 32x32 samples. Two consecutive spectrograms are shifted in time with a lag of 1.0 s [24]. Each spectrogram is then compressed applying the Haar wavelet transform and maintaining only the 200 out of 1024 coefficients that most detach from their daily average. This compression is shown to preserve the seismic features in the fingerprints under the assumption that the daily average is representative of the ambient noise. The selected coefficients are then binarized, following the scheme of Yoon et al., (2015) to generate final fingerprints, each consisting of 2048 bits.

In the similarity search step (Block 3 of Figure 3), FAST uses the Jaccard similarity to compare the fingerprints. Such a comparison is reduced to a limited number of fingerprint characteristics extracted through the application of a Min-Hash independent permutation algorithm [36]. In the bottom panels (a) and (b) of Figure 3 waveforms from two events (14 and 15 in Table 1) and the associated fingerprints are plotted. The shown fingerprints are characterized by a high Jaccard similarity, and hence will be inspected at following steps for event declaration.

The fingerprint pairs extracted at component level are combined together and associated at the network level allowing time delays compatible with the wave propagation within the network (Figure 3 Block 4 and panel c). At this stage, we select transients only if their similarity is retrieved at least at 4 stations. The transient list is further investigated in terms of first arrival times and duration. For the Collalto array, several candidate events forming a family of candidate events were removed because of low apparent velocity across the array, long duration and almost monochromatic character. These characteristics let us guess that such transients were related to anthropic activity and/or weather effects. Finally, local earthquakes from regional and teleseismic events separation is carried out according to the transients' duration. After this last step, the catalogue was further enhanced including all the transients associated at less than 4 stations but being similar at least at 2 stations. The final catalogue provided by FAST is a detection list without locations. Some of the detected events are reported in the RSC catalogue for the larger events (hereinafter, reference events). This information concerning the reference events is used, hence, to assume that smaller events featuring low signal-to-noise ratio and belonging to the same family of the larger ones are co-located with them.

For those small events that were declared similar to an event included in the RSC catalogue, we computed the magnitude of these latter events as:

$$Ml = Ml_{ref} + \log_{10} \left(\frac{A}{A_{ref}} \right) \quad (1)$$

where A is the maximum peak-to-peak displacement amplitude on the non-filtered horizontal components of the target event while Ml_{ref} and A_{ref} are the magnitude and the maximum peak-to-peak displacement amplitude of reference event respectively. The magnitude values obtained at the stations where FAST declared the similarity are then averaged to obtain the final estimation.

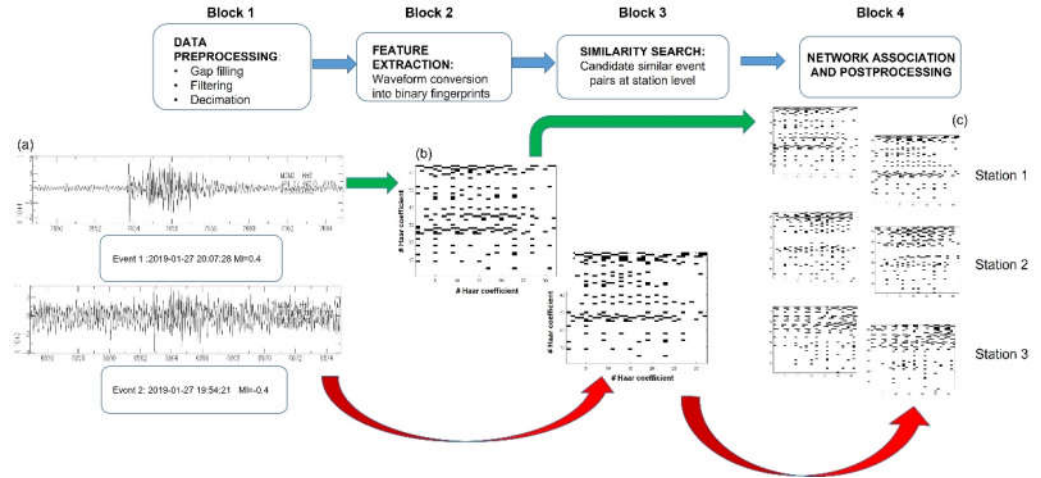


Figure 3. Top, with blue arrows: Workflow of the FAST data processing for microseismicity detection. Bottom: an application example based on two events included in the Table 1 (see section 4)

4. Results

We applied the analysis described in section 3 and detected 38 transients. Among them, 20 transients were discarded during the post-processing association phase due to unrealistic apparent velocity within the array. Indeed, they are characterized by signals having short durations ($t_d < 20s$) and large difference between the arrival times at the different array nodes ($\max \{t_0^j - t_0^i\} > 10s$). For verifying the algorithm performance, we visually inspected them, and we confirmed that these waveforms were not seismic signals being characterized by either monochromatic wave trains or superposition of two monochromatic components at close frequencies. At the end of the analysis, we obtained a list of 18 detections.

It is worth to highlight that, during the experiment, a seismic sequence occurred in the district of Ravenna, at an epicentral distance of about 230 km from the array centre, with the largest event having magnitude Mw 4.3. Inspecting the detected events, FAST declared 5 different transients that can be associated with 3 events of this sequence. The number of transients (5) is larger than the associated events (3) since two events were detected twice (FAST separately declared P-waves and later surface waves).

Our final catalogue is composed of 16 seismic events (Table 1). These events are ordered according to their origin time, and with the associated location and magnitude as extracted from the INGV or the RCS catalogue, when available. The last column of Table 1 indicates the events, to which FAST declared the similarity.

We recognize 7 local events that occurred in the area of Collalto, while the remaining ones are regional or teleseismic events.

Table 1. Final catalogue from the application of the FAST analysis to the array continuous data

Event n.	Date/Time UTC	Latitude	Longitude	Depth (km)	Place	Triggered stations	Magnitude	Agency Amp. Ratio (AR)	Similarity
01	2019-01-10 18:42:12	46.842	11.198	12	Bolzano, Italy	6	2.7 (MI)	INGV	02 – 11
02	2019-01-13 08:33:07	46.224	12.376	6	Belluno, Italy	7	2.4 (MI)	INGV	01 – 11
03	2019-01-14 20:32:21	N/A	N/A	N/A	Conegliano, Italy	4	-0.4 (MI)	AR - Ev.09	09
04	2019-01-14 22:10:18	N/A	N/A	N/A	Conegliano, Italy	4	-0.2 (MI)	AR - Ev.09	09
05	2019-01-14 23:03:57	44.347	12.286	21	Ravenna, Italy	8	4.3 (Mw)	INGV	06 – 07
06	2019-01-14 23:29:07	44.377	12.302	21	Ravenna, Italy	8	3.0 (MI)	INGV	05 – 07
07	2019-01-15 00:45:41	44.292	12.23	15	Ravenna, Italy	8	2.0 (MI)	INGV	05 – 06
08	2019-01-15 01:25:05	38.93	20.55	10	Greece	5	4.5 (mb)	EMSC	12 – 16
09	2019-01-15 12:05:20	45.904	12.218	7.9	Conegliano, Italy	7	0.1 (MI)	OGS	04 – 05 – 10 – 15
10	2019-01-15 17:26:44	45.893	12.208	8.4	Conegliano, Italy	7	0.0 (MI)	OGS	09 – 15
11	2019-01-15 18:31:04	46.419	13.173	14	Udine, Italy	4	2.4 (MI)	INGV	01 – 02
12	2019-01-26 19:56:43	-21.206	-178.716	594	Fiji Islands	4	6.1 (Mwp)	EMSC	08 – 16
13	2019-01-27 13:51:37	N/A	N/A	N/A	Vittorio Veneto, Italy	2	-0.4 (MI)	AR - Event 15	15
14	2019-01-27 19:54:21	N/A	N/A	N/A	Vittorio Veneto, Italy	3	-0.4 (MI)	AR - Event 15	15
15	2019-01-27 20:07:31	45.935	12.238	8.7	Vittorio Veneto, Italy	6	0.4 (MI)	OGS	09 – 10
16	2019-01-29 12:53:45	51.58	16.10	10	Poland	6	4.8 (mb)	EMSC	08 - 12

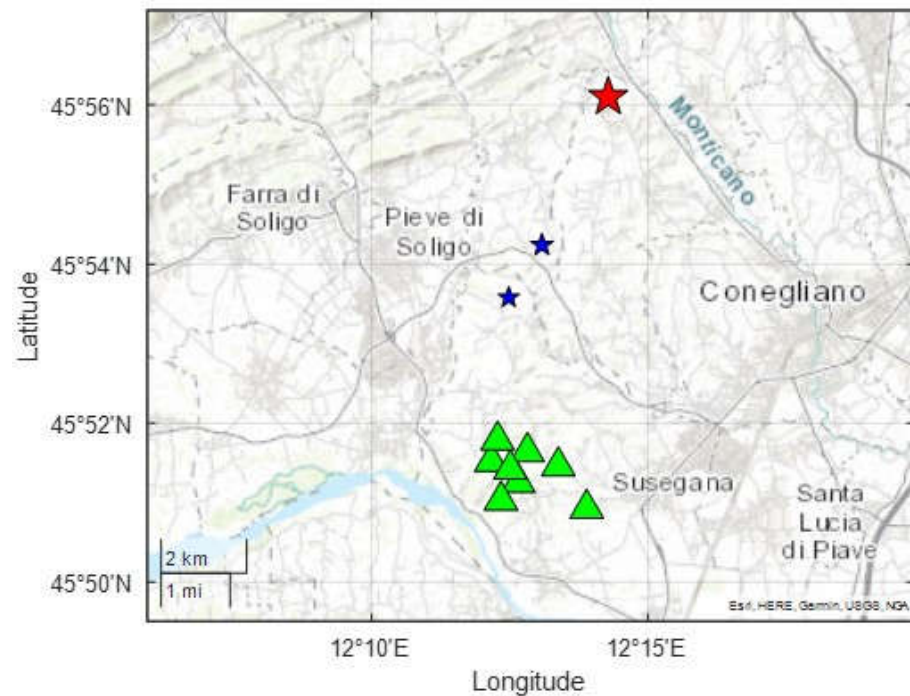


Figure 4. – Location of the events detected by FAST and included in the OGS catalogue in the vicinity of the array. Blue stars represent the events 9 and 10 in Table 1, while the red star represents the event 15 in Table 1. The size of the stars is proportional to the magnitude of the events and the green triangles mark the position of the array stations.

The three events belonging to the Ravenna sequence (ev. number 05-06-07 in Table 1) were detected because their waveforms were similar to each other (Figure S1 in the Supplementary Material). The same condition holds for three regional events (ev. 01-02-11 in Table 1, Figure S2 in the Supplementary Material) originated northward of the array at distances ranging from ~45 to ~135 km, and for three teleseisms (ev. 08-12-16 in Table 1, Figure S3 in the Supplementary Material). These latter events were declared due to the similarity in the frequency content of surface waves recorded at the array stations, within the sampled frequency band.

Concerning the local events, we found two detections located close to Conegliano (ev. 09-10 in Table 1, blue stars in Figure 4, Figure S4c-d in Supplementary Material). These latter were the closest earthquakes to the array that occurred during the experiment, according to the RCS catalogue, with magnitude M_l 0.1 and M_l 0.0 respectively. Other two events were detected by FAST (ev. 03-04 in Table 1, Figure S4a-b in the Supplementary Material) not reported in the catalogue. These events were declared because of their reciprocal similarity and their similarity with ev. 09. They feature a very low signal-to-noise ratio ($SNR \sim 1.5$) and cannot be located using the array records. However, considering that their waveforms are very similar with those of the ev. 09, we assumed these events co-located and provided an estimate of the magnitude (M_l -0.4 and -0.2 respectively) as the average magnitude value computed by applying the equation (1) at all the stations where the events were declared. In the following, we will discuss the performance of FAST in terms of minimum detectable magnitude in the area close to the Collalto gas storage area and the meaning itself of the local magnitude scale for such small events.

In addition, FAST correctly identified also the M_l 0.4 event located at Vittorio Veneto (ev. 15 in Table 1, red star in Figure 4), which was also included in the RCS catalogue and two further events (ev. 13-14, Figure S5 in the Supplementary Material), similar to it. Also in this case, the magnitude was estimated through the amplitude ratio (eq.) considering the ev. 15 as a reference.

It is worth noting that the negative magnitude events of Conegliano (ev. 03-04 in Table 1) and Vittorio Veneto (ev. 13-14 in Table 1) anticipated the corresponding larger-magnitude events; in particular the events 03 and 04 occurred ~15.5 and ~14 hours before the event 09, while the events 13 and 14 were detected ~6.5 hours and ~13 minutes before the origin time of event 15. We finally highlight that for the whole period of our experiment, no events located in the close vicinity of the array and gas-storage were detected.

5. Discussion

The similarity search results do not report any detected earthquake nearby the gas storage during the experiment. Nevertheless, the procedure allowed us to detect 7 events a few kilometers apart from the array deployment towards north, 4 of which represent new events. For the new detections, we exploited their high similarity to some larger-magnitude events, so that we co-located the new small events with the corresponding parents and estimated their magnitude, which resulted to be negative. Despite the small number of these new events, we can interpret them as foreshocks of the two larger-magnitude reference events. According to [37], who observed foreshocks before small magnitude events in Central Alaska, a systematic observation of foreshocks associated with small magnitude events for long periods could help to investigate the continuity and complexity of slip processes occurring in a specific area. Our results, hence, suggest that the integration of seismic networks and seismic arrays over long periods, combined with advanced data analysis strategies could help to shed light on important questions concerning the earthquake nucleation.

The limited duration of our experiment did not allow us to fully estimate the capability of the full permanent and temporary deployment in monitoring the micro-seismicity with respect to the storage area target. However, starting from our results, in the following we propose a strategy to i) infer the smallest magnitude that could have been detected in the study area; ii) confirm, within a fixed level of confidence, that no events above a certain level of magnitude occurred in the gas-storage area during the experiment period.

To estimate the minimum magnitude that could have been detected in the storage area, we investigate the noise distribution in the waveforms processed through the similarity search of FAST. For this study, the data stream at all stations of the array was subdivided into one-minute-long windows and then filtered in the band 1-20 Hz, similarly to the pre-processing phase described in section 3. Within each window, the level of noise was estimated as the RMS of the whole signal. Figure 5 shows the empirical cumulative distribution of the noise along with the level corresponding to the 90th percentile, that is $1.08 \cdot 10^{-6} \text{ m/s}$.

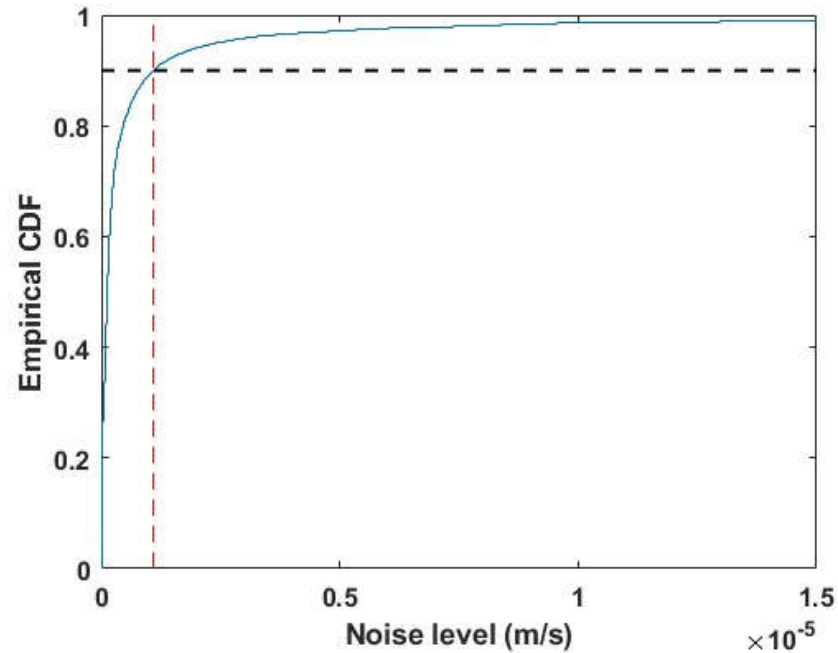


Figure 5. Empirical Cumulative Distribution Function (ECDF) of the noise distribution. The horizontal black dashed line marks the 0.9 level and the red dashed line intercepts the 90th percentile for the distribution.

For local events detected by FAST, we computed the signal-to-noise ratio (SNR) on the horizontal components of the stations associated by FAST. Considering 7 seconds-long windows before and after the origin time as the noise $N(t)$ and the signal $S(t)$ contributions, we computed the Fourier transforms of both time series $N(\nu)$ and $S(\nu)$. The SNR writes as:

$$SNR = \frac{\int_{f_1}^{f_2} \hat{S}(\nu) d\nu}{\int_{f_1}^{f_2} \hat{N}(\nu) d\nu} \quad (2)$$

where, $f_1 = 1\text{Hz}$ and $f_2 = 20\text{Hz}$. For the 3 largest events of the two clusters (ev. 9, 10 and 15 in Table 1) SNR ranges between 4 and 6 at all the horizontal components of the stations of the array, while for the smallest ones (ev. 3, 4, 13 and 14 in Table 1) SNR ranges between 1.01 and 1.67 with a mean value $\langle \text{SNR} \rangle = 1.34$. We can consider this mean value as an estimate of the limit for the detection capability of the array system processed by FAST. Around this $\langle \text{SNR} \rangle$ level, we have detected events of minimum magnitude $M = -0.4$ at a maximum hypocentral distance $R = 13$ km. Fixing this SNR level and reducing the distance in the range between 2 km and 3 km, to account for events potentially occurring nearby the gas-storage area, we can estimate the minimum detectable magnitude using the local magnitude scaling law proposed by [38] and valid for North-eastern Italy:

$$Ml(r) = \log_{10} A + n \log_{10} \left(\frac{r}{R^*} \right) + k(r - R^*) - 3 + S \quad (3)$$

with Ml local magnitude, $n = 1$, $k = 0.0169\text{km}^{-1}$, r the distance (in km), $R^* = 100\text{km}$, S the local station coefficient, which is assumed zero, and A the Wood-Anderson displacement maximum amplitude. To estimate the limit magnitude detectable around the array deployment, considering the overall level of noise and the estimated quantity $\langle \text{SNR} \rangle$, we replace the amplitude term, in equation (3) with the following quantity:

$$A_{\text{over-noise}} = \langle \text{SNR} \rangle \cdot A_n^{\text{noise}} \quad (4)$$

with A_n^{noise} the Wood-Anderson amplitude of the n th percentile of the noise distribution (see Figure 5). Equations (3) and (4) enable the magnitude estimate for a local event located at a generic distance r , generating an amplitude emerging from a fixed level of noise with a prescribed SNR level. The higher the percentile the more our estimate represents a good proxy for the magnitude of completeness of the system.

The results of this analysis using a value of $\langle \text{SNR} \rangle = 1.34$ for computing equations (3) and (4) are shown in Figure 6 for different percentile values of the noise amplitude. Considering that the Collalto gas-storage has an average depth of 1.5-1.6 km, and taking into account a range of reference distances between 2 km and 3 km from the array stations, we have retrieved an average limit magnitude Ml_{lim} between -0.8 and -0.6 when we select a noise level equal to the 90th percentile of the noise distribution. Thus, we can state, with a 90% level of confidence, that no events with local magnitude larger than -0.6 have occurred within the study area during the experiment.

All the estimated magnitudes presented here are local magnitudes derived from the regional scaling presented in [38]. The values discussed in this study are small and well below the limit for which the local magnitude Ml can be estimated without systematic bias. (e.g. [9,39]). This is due to the restriction of the exploitable frequency range for the analysis, determined by the sampling rate generally adopted by the networks (low compared to frequency content of the micro earthquakes), the signal to noise ratio and the combined effect of the anelastic and scattering attenuation [40-41]. This implies any interpretation of the local magnitude in terms of seismic moment should be treated with caution. Indeed, when decreasing the magnitude, the corner frequency is above the Nyquist frequency providing a theoretically faster scaling for the local magnitude than for larger earthquakes [41].

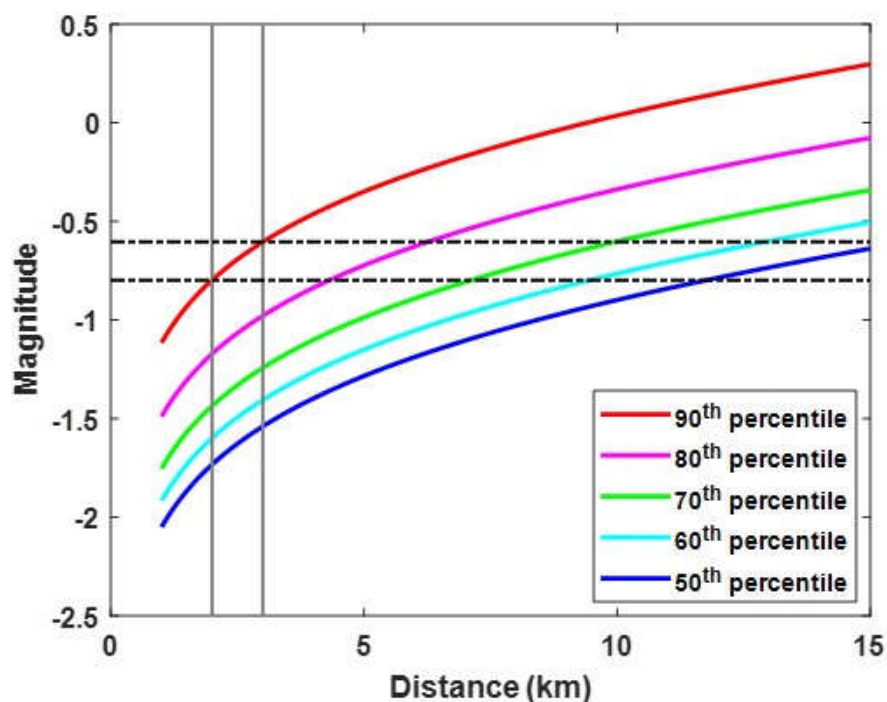


Figure 6. Attenuation curves computed through the application of equation . The coloured solid lines represent the different percentiles of the noise distribution as reported in the legend. The grey solid lines mark the reference distance range between 2 and 3 km, while the dashed-dotted black lines represent the average limit magnitude at those distances for the 90th percentile curve.

To provide a theoretical interpretation of the results and estimate to what extent the improvement is due to the proposed seismic array technique, we followed the approach of [4]. Considering the seismic noise conditions observed during the experiment, we evaluated the expected detection capability of the Collalto standard network integrated with the seismic array for events at 2.5 km depth. For the simulation, we have considered the scenario composed by the Collalto seismic network integrated with the array, the noise level evaluated in this study ($\sim 10^{-6}$ m/s), and the 1D local velocity derived for the area [42-43]. Figure 7(a) shows that for an area of 2-3 km around the reservoir the minimum expected detectable magnitude is approximately 0.0. It is worth noting that the detection threshold adopted in this analysis is estimated by considering a standard detection technique based on STA/LTA requiring a $SNR > 4$ for at least three S-wave phases. Concerning these detection criteria, we observe no significant improvement of the RSC magnitude of completeness, obtained from visual waveform inspection [10]. When using the same waveforms similarity criteria as adopted for FAST processing and a threshold of $SNR > 1.5$, the expected magnitude of completeness improved to -0.7, consistent with the M_{lim} estimated above. In this framework, the main contribution of a dense seismic array placed in the close vicinity of the gas storage area is to increase the number of stations where the minimum needed SNR is achieved.

In conclusion, also taking into account all the described limitations, our findings suggest that the empirical estimation presented in Figure (6) is a good proxy of the magnitude of completeness of the experimental system and that, in this configuration, most of the improvement results from the application of an efficient detection algorithm based on similarity-search, that allows us to catch events with amplitude comparable to the noise level.

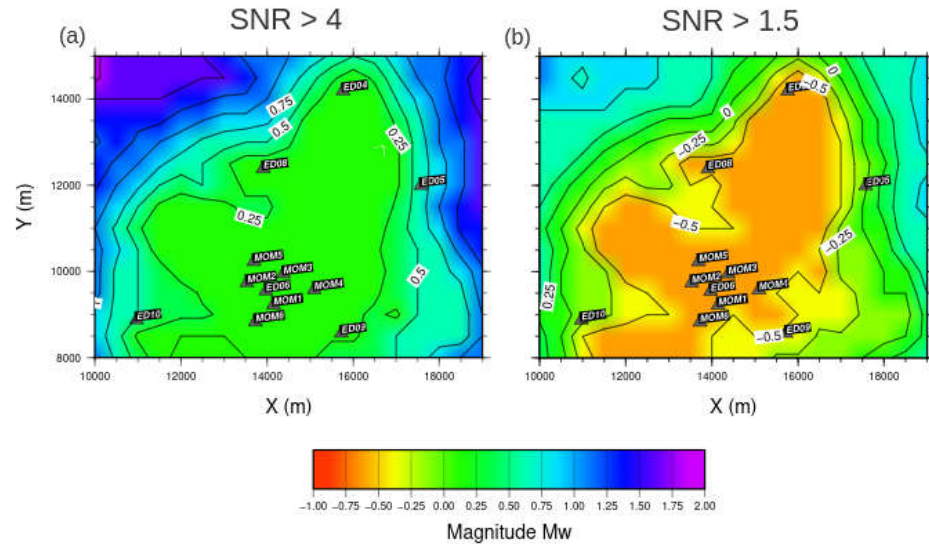


Figure 7. Map of the theoretical minimum detectable magnitude for the array+RSC network configuration considering SNR for the detection at least 4 (a) and at least 1.5 (b).

6. Conclusions

This work is grounded on a monitoring experiment carried out in the Collalto gas-storage area in the North-East of Italy. Here, we installed a seismic array with a radius smaller than 2 km, and analysed continuous velocity data acquired for 25 days during wintertime through the application of the optimized auto-similarity search technique FAST. The array monitoring system was conceived as a low-cost system, aimed at integrating the permanent high-resolution Collalto Seismic Network (Rete Sismica Collalto, RSC) right above the gas storage site.

FAST was able to detect all the small events included in the RSC earthquake catalogue and occurred just outside the gas-storage area, within a distance of 15 km from the array. These events were very small, and their magnitude was in the range 0.0 – 0.4, very close to the magnitude of completeness of the RSC network. FAST was also able to detect 4 more events, all with negative magnitude and not reported in the RSC catalogue, which occurred a few hours before the reference events. Instead, no event were detected right below the array or the gas storage area.

To infer the detection capability of the system, we first defined a proxy for the minimum SNR enabling the detection by estimating the overall distribution of the signal-to-noise ratio for the smallest detected events throughout the array. This SNR threshold resulted, on average, equal to 1.34, revealing that the system was able to detect micro-earthquake whose signals were fully buried in the noise. The overall noise amplitude distribution and the minimum SNR estimates were in turn used to quantify the minimum magnitude that could be detected for events occurring in the gas-storage area. Exploiting the magnitude law proposed for North-East Italy by [38], and considering the 90th percentile of the noise distribution, the limit magnitude of detectable events ranges between -0.8 and -0.6. Thus, we can also reasonably guess that no events with occurred during the experiment within the gas-storage area. These findings are consistent with the theoretical model proposed by [4], which indicates that most of the improvements is due to the application of an advanced data-mining strategy enabling detection of events even with very low SNR.

Supplementary Materials: The following supporting information can be downloaded at: www.mdpi.com/xxx/s1, Figure S1-S5: Signals of detected events collected by similarity.

Author Contributions: A.S., G.M.A. and M.P. managed the workflow from experiment conceptualization to the manuscript preparation. R.R., M.R.G.M.A., M.P., S.P., and E.P., worked to the organization and realization of the field experiment. A.S., F.S.d.U. and G.F. worked to the data analysis and catalogue definition. A.S., G.M.A., M.P., F.S.d.U., G.F., S.P., E.P. and G.D.L contributed to the results discussion and interpretation. All authors contributed to the preparation of the manuscript and revised it several times.

Acknowledgments: The Collalto Seismic Network is managed by the OGS on behalf of Edison Stocaggio S.p.A., under requirements of the Italian Ministry for the Environment, Land, and Sea Protection (MATTM) and in agreement with the Veneto Region. The authors acknowledge the full cooperation of Edison Stocaggio S.p.A. in achieving the objectives of this research.

Conflicts of Interest: The authors declare no conflict of interest.

References

1. Ellsworth, W.L. Injection-Induced Earthquakes. *Science* **2013**, Vol 341, Issue 6142. <https://doi.org/10.1126/science.1225942>.
2. Goertz-Allmann, B. P., Goertz, A., & Wiemer, S. Stress drop variations of induced earthquakes at the Basel geothermal site. *Geophys. Res. Lett.* **2011**, 38(9). <https://doi.org/10.1029/2011gl047498>
3. Grigoli, F., Cesca, S., Priolo, E., Rinaldi, A. P., Clinton, J. F., Stabile, T. A., Dost, B., Fernandez, M. G., Wiemer, S., & Dahm, T. Current challenges in monitoring, discrimination, and management of induced seismicity related to underground industrial activities: A European perspective. *Rev. of Geophys.*, **2017**, 55(2), 310–340. <https://doi.org/10.1002/2016RG000542>.
4. De Landro, G., Picozzi, M., Russo, G., Adinolfi, G. M., and Zollo, A. Seismic networks layout optimization for a high-resolution monitoring of induced micro-seismicity. *J. of Seism.* **2020**, 24(5), 953–966. <https://doi.org/10.1007/s10950-019-09880-9>.
5. MiSE. Guidelines For Monitoring Seismicity, Ground Deformation And Pore Pressure In Subsurface Industrial Activities. **2014**. Available online: https://unmig.mise.gov.it/images/docs/151_238.pdf (accessed on 23 march 2022).
6. Priolo, E., Romanelli, M., Plasencia Linares, M. P., Garbin, M., Peruzza, L., Romano, M. A., Marotta, P., Bernardi, P., Moratto, L., Zuliani, D., and Fabris, P. Seismic monitoring of an underground natural gas storage facility: The Collalto seismic network. *Seism. Res. Lett.*, **2015** Vol. 86(1), 109–123. <https://doi.org/10.1785/0220140087>.
7. Centrale Stoccaggio di Collalto. Available online : <https://www.edison.it/it/centrale-stoccaggio-di-collalto> (accessed on 23 march 2022)
8. Romano, M. A., Peruzza, L., Garbin, M., Priolo, E., and Picotti, V. Microseismic Portrait of the Montello Thrust (Southeastern Alps, Italy) from a Dense High-Quality Seismic Network. *Seism. Res. Lett.* **2019**, Vol. 90 (4): 1502–1517. <https://doi.org/10.1785/0220180387>.
9. Lanzoni, A., Moratto, L., Priolo, E., and Romano, M. A. Fast MW estimation of microearthquakes recorded around the underground gas storage in the Montello-Collalto area (Southeastern Alps, Italy). *J. of Seism.* **2020**, Vol. 24(5), 1029–1043. <https://doi.org/10.1007/s10950-019-09889-0>.
10. Priolo E. et al. Rete di rilevamento sismico finalizzata al monitoraggio della sismicità naturale e microsismicità indotta presso la concessione di stoccaggio gas metano denominata “Collalto Stoccaggio” (TV) **2021** - Prima relazione annuale.
11. Gibbons, S. J., and Ringdal, F. The detection of low magnitude seismic events using array-based waveform correlation. *Geophys. J. Int.*, 2006, Vol. 165(1), 149–166. <https://doi.org/10.1111/j.1365-246X.2006.02865.x>.
12. Peng, Z., and Zhao, P. Migration of early aftershocks following the 2004 Parkfield earthquake. *Nat. Geo.*, **2009** Vol. 2(12), 877–881. <https://doi.org/10.1038/ngeo697>.
13. Barrett, S. A., and Beroza, G. C. An Empirical Approach to Subspace Detection. *Seism. Res. Lett.*, **2014** Vol. 85(3), 594–600. <https://doi.org/10.1785/0220130152>.
14. Chamberlain, C. J., Townend, J., and Gerstenberger, M. C. RT-EQcorrscan: Near-Real-Time Matched-Filtering for Rapid Development of Dense Earthquake Catalogs. *Seism. Res. Lett.*, **2020** Vol. 91(6), 3574–3584. <https://doi.org/10.1785/0220200171>.
15. Cesca, S., Stich, D., Grigoli, F., Vuan, A., López-Comino, J. Á., Niemi, P., Blanch, E., Dahm, T., & Ellsworth, W. L. Seismicity at the Castor gas reservoir driven by pore pressure diffusion and asperities loading. *Nat. Comm.*, **2021** Vol. 12(1). <https://doi.org/10.1038/s41467-021-24949-1>.
16. Mousavi, S. M., Ellsworth, W. L., Zhu, W., Chuang, L. Y., and Beroza, G. C. Earthquake transformer—an attentive deep-learning model for simultaneous earthquake detection and phase picking. *Nat. Comm.*, **2020** Vol. 11(1), 3952. <https://doi.org/10.1038/s41467-020-17591-w>.
17. Parolai, S., Trojani, L., Frapiccini, M., and Monachesi, G. Seismic Source Classification by Means of a Sonogram- Correlation Approach: Application to Data of the RSM Seismic Network (Central Italy). *Pure Appl. Geophys.*, **2002** Vol. 159(11–12), 2763–2788. <https://doi.org/10.1007/s00024-002-8758-z>.
18. Brown, J. R., Beroza, G. C., and Shelly, D. R. An autocorrelation method to detect low frequency earthquakes within tremor. *Geophys. Res. Lett.*, **2008** Vol. 35(16), L16305. <https://doi.org/10.1029/2008GL034560>.
19. Poiata, N., Satriano, C., Vilotte, J.-P., Bernard, P., & Obara, K. Multiband array detection and location of seismic sources recorded by dense seismic networks. *Geophys. J. Int.*, **2016** Vol. 205(3), 1548–1573. <https://doi.org/10.1093/gji/ggw071>.
20. Skoumal, R. J., Brudzinski, M. R., and Currie, B. S. An efficient repeating signal detector to investigate earthquake swarms. *J. Geophys. Res.-Sol. Ea.*, **2016** Vol. 121(8), 5880–5897. <https://doi.org/10.1002/2016JB012981>.
21. Guidarelli, M., Klin, P., and Priolo, E. Migration-based near real-time detection and location of microearthquakes with parallel computing. *Geophys. J. Int.*, **2020** Vol. 221(3), 1941–1958. <https://doi.org/10.1093/gji/ggaa111>.
22. Yoon, C. E., O'Reilly, O., Bergen, K. J., and Beroza, G. C. Earthquake detection through computationally efficient similarity search. *Sc. Adv.*, **2015** Vol. 1(11). <https://doi.org/10.1126/sciadv.1501057>.
23. Bergen, K. J., & Beroza, G. C. Detecting earthquakes over a seismic network using single-station similarity measures. *Geophys. J. Int.*, **2018**, Vol. 213(3), 1984–1998. <https://doi.org/10.1093/gji/ggy100>.

24. Yoon, C. E., Yoshimitsu, N., Ellsworth, W. L., and Beroza, G. C. Foreshocks and Mainshock Nucleation of the 1999 M_w 7.1 Hector Mine, California, Earthquake. *J. Geophys. Res.- Sol. Ea.*, **2019**, Vol. 124(2), 1569–1582. <https://doi.org/10.1029/2018JB016383>.
25. Vassallo, M., Festa, G., and Bobbio, A. Seismic Ambient Noise Analysis in Southern Italy. *Bull. Seism. Soc. Am.*, **2012** Vol. 102(2), 574–586. <https://doi.org/10.1785/0120110018>.
26. Festa, G., Adinolfi, G. M., Caruso, A., Colombelli, S., de Landro, G., Elia, L., Emolo, A., Picozzi, M., Scala, A., Carotenuto, F., Gammaldi, S., Iaccarino, A. G., Nazeri, S., Riccio, R., Russo, G., Tarantino, S., and Zollo, A. Insights into Mechanical Properties of the 1980 Irpinia Fault System from the Analysis of a Seismic Sequence. *Geosci.*, **2021** Vol. 11(1), 28. <https://doi.org/10.3390/geosciences11010028>.
27. Castellarin, A., Nicolich, R., Fantoni, R., Cantelli, L., Sella, M., and Selli, L. Structure of the lithosphere beneath the Eastern Alps (southern sector of the TRANSALP transect). *Tectonophysics*, **2006** Vol. 414, (1–4). <https://doi.org/10.1016/j.tecto.2005.10.013>.
28. Burrato, P., Poli, M. E., Vannoli, P., Zanferrari, A., Basili, R., and Galadini, F. Sources of Mw 5+ earthquakes in northeastern Italy and western Slovenia: An updated view based on geological and seismological evidence. *Tectonophysics*, **2008**, Vol. 453(1–4). <https://doi.org/10.1016/j.tecto.2007.07.009>.
29. Castellarin, A., and Cantelli, L. Neo-Alpine evolution of the Southern Eastern Alps. *J. of Geodyn.*, **2000**, Vol. 30(1–2). [https://doi.org/10.1016/S0264-3707\(99\)00036-8](https://doi.org/10.1016/S0264-3707(99)00036-8).
30. Mellere D., Stefani C., and Angevine C. Polyphase Tectonics through subsidence analysis: the Oligo-Miocene Venetian and Friuli Basin, north-east Italy. *Bas. Res.*, **2000**, Vol. 12(2). <https://doi.org/10.1046/j.1365-2117.2000.00120.x>.
31. Serpelloni, E., Vannucci, G., Anderlini, L., and Bennett, R. A. Kinematics, seismotectonics and seismic potential of the eastern sector of the European Alps from GPS and seismic deformation data. *Tectonophysics*, **2016** Vol. 688. <https://doi.org/10.1016/j.tecto.2016.09.026>.
32. Rovida, A., Locati, M., Camassi, R., Lolli, B., Gasperini, P., Antonucci, A., Azzaro, R., Bernardini, F., D'Amico, S., Ercolani, E., Rossi, A., Tertulliani, A., Meletti, C., Albini, P., Castelli, V., Caracciolo, C. H., Amico, V. D. ', Pondrelli, S., and Rebez, A.. Italian Parametric Earthquake Catalogue CPTI15 version 4.0 macroseismic data management and validation, **2016**. Available online: <https://doi.org/10.13127/cpti/cpti15.4> (accessed on 23 march 2022)
33. Galadini, F., Poli, M. E., and Zanferrari, A. Seismogenic sources potentially responsible for earthquakes with M ≥ 6 in the eastern Southern Alps (Thiene-Udine sector, NE Italy). *Geophysical Journal International*, **2005**, 161(3). <https://doi.org/10.1111/j.1365-246X.2005.02571.x>.
34. Poli, M. E., Burrato, P., Galadini, F., and Zanferrari, A. Seismogenic sources responsible for destructive earthquakes in north-eastern Italy. *B. Geofis. Teor. Appl.*, **2008**, Vol. 49, (3-4), pp. 301-313.
35. Barba, S., Finocchio, D., Sikdar, E., and Burrato, P. Modelling the interseismic deformation of a thrust system: seismogenic potential of the Southern Alps. *Terra Nova*, **2013**, Vol. 25(3). <https://doi.org/10.1111/ter.12026>.
36. Broder, A. Z., Charikar, M., Frieze, A. M., & Mitzenmacher, M. Min-Wise Independent Permutations, **2000**. Available online: <https://www.cs.princeton.edu/courses/archive/spr04/cos598B/bib/BroderCFM-minwise.pdf> (accessed on 23 march 2022).
37. Tape, C., Holtkamp, S., Silwal, V., Hawthorne, J., Kaneko, Y., Ampuero, J.-P., Ji, C., Ruppert, N., Smith, K., and West, M. E. Earthquake nucleation and fault slip complexity in the lower crust of central Alaska. *Nat. Geosci.*, **2018**, 11, 536–541 (2018). <https://doi.org/10.1038/s41561-018-0144-2>.
38. Bragato, P. L., and Tiento, A. Local magnitude in northeastern Italy. *Bull. Seism. Soc. Am.*, **2005** Vol. 95(2), 579–591. <https://doi.org/10.1785/0120040100>.
39. Moratto, L., Saraò, A., and Priolo, E. Moment magnitude (M_w) estimation of weak seismicity in Northeastern Italy. *Seismol. Res. Lett.*, **2017**, Vol. 88(6), 1455-1464. <https://doi.org/10.1785/0220170063>.
40. Deichmann, N. Local Magnitude, a Moment Revisited. *Bull. Seism. Soc. Am.*, **2006**, Vol. 96(4A). <https://doi.org/10.1785/0120050115>.

-
41. Deichmann, N. Theoretical Basis for the Observed Break in M_L / M_w Scaling between Small and Large Earthquakes. *Bull. Seism. Soc. Am.*, **2017**, Vol. 107(2). <https://doi.org/10.1785/0120160318>.
 42. Priolo, E., Barnaba, C., Bernardi, P., Bernardis, G., Bragato, P. L., Bressan, G., Candido, M., Cazzador, E., di Bartolomeo, P., Duri, G., Gentili, S., Govoni, A., Klinc, P., Kravanja, S., Laurenzano, G., Lovisa, L., Marotta, P., Michelini, A., Ponton, F., Restivo A., Romanelli M., Snidarcig A., Urban S., Vuan A., and Zuliani D. Seismic Monitoring in Northeastern Italy: A Ten-year Experience. *Seism. Res. Lett.*, **2005** Vol. 76(4), 446–454. <https://doi.org/10.1785/gssrl.76.4.446>.
 43. Bragato, P. L., di Bartolomeo, P., Pesaresi, D., Percy, M., and Saraò, A. Acquiring, archiving, analyzing and exchanging seismic data in real time at the Seismological Research Center of the OGS in Italy. *Ann. Geophys.*, 2011, Vol. 54(1). <https://doi.org/10.4401/ag-4958>